

Mg-doped layered oxide cathode for Na-ion batteries

Yuejun Ding(丁月君), Feixiang Ding(丁飞翔), Xiaohui Rong(容晓晖), Yaxiang Lu(陆雅翔), and Yong-Sheng Hu(胡勇胜)

Citation: Chin. Phys. B, 2022, 31 (**6**): 068201. DOI: 10.1088/1674-1056/ac523b
Journal homepage: http://cpb.iphy.ac.cn; http://iopscience.iop.org/cpb

What follows is a list of articles you may be interested in

Lithium ion batteries cathode material: V_2O_5

Baohe Yuan(袁保合), Xiang Yuan(袁祥), Binger Zhang(张冰儿), Zheng An(安政), Shijun Luo(罗世钧), and Lulu Chen(陈露露)

Chin. Phys. B, 2022, 31 (**3**): 038203. DOI: 10.1088/1674-1056/ac21be

In situ formed FeS_2@CoS cathode for long cycling life lithium-ion battery

Xin Wang(王鑫), Bojun Wang(汪博筠), Jiachao Yang(杨家超), Qiwen Ran(冉淇文), Jian Zou(邹剑), Pengyu Chen(陈鹏宇), Li Li(李莉), Liping Wang(王丽平), and Xiaobin Niu(牛晓滨)

Chin. Phys. B, 2021, 30 (**8**): 088201. DOI: 10.1088/1674-1056/abe9ab

Electron density distribution of $LiMn_2O_4$ cathode investigated by synchrotron powder x-ray diffraction

Tongtong Shang(尚彤彤), Dongdong Xiao(肖东东), Qinghua Zhang(张庆华), Xuefeng Wang(王雪锋), Dong Su(苏东), and Lin Gu(谷林)

Chin. Phys. B, 2021, 30 (**7**): 078202. DOI: 10.1088/1674-1056/abf347

New layered metal oxides as positive electrode materials for room-temperature sodium-ion batteries

Mu Lin-Qin, Hu Yong-Sheng, Chen Li-Quan

Chin. Phys. B, 2015, 24 (**3**): 038202. DOI: 10.1088/1674-1056/24/3/038202

Novel copper redox-based cathode materials for room-temperature sodium-ion batteries

Xu Shu-Yin, Wu Xiao-Yan, Li Yun-Ming, Hu Yong-Sheng, Chen Li-Quan

Chin. Phys. B, 2014, 23 (**11**): 118202. DOI: 10.1088/1674-1056/23/11/118202

RAPID COMMUNICATION

Mg-doped layered oxide cathode for Na-ion batteries

Yuejun Ding(丁月君)[1,2], Feixiang Ding(丁飞翔)[1], Xiaohui Rong(容晓晖)[1,†], Yaxiang Lu(陆雅翔)[1], and Yong-Sheng Hu(胡勇胜)[1,2,‡]

[1] *Key Laboratory for Renewable Energy, Beijing Key Laboratory for New Energy Materials and Devices, Beijing National Laboratory for Condensed Matter Physics, Institute of Physics, Chinese Academy of Sciences, Beijing* 100190, *China*

[2] *Center of Materials Science and Optoelectronics Engineering University of Chinese Academy of Sciences, Beijing* 100190, *China*

(Received 26 November 2021; revised manuscript received 1 December 2021; accepted manuscript online 7 February 2022)

Na-ion batteries (NIBs) are regarding as the optimum complement for Li-ion batteries along with the rapid development of stationary energy storage systems. In order to meet the commercial demands of cathodes for NIBs, O3-type Cu containing layered oxide $Na_{0.90}Cu_{0.22}Fe_{0.30}Mn_{0.48}O_2$ with good comprehensive performance and low-cost element components is very promising for the practical use. However, only part of the Cu^{3+}/Cu^{2+} redox couple participated in the redox reaction, thus impairing the specific capacity of the cathode materials. Herein, Mg^{2+}-doped O3-$Na_{0.90}Mg_{0.08}Cu_{0.22}Fe_{0.30}Mn_{0.40}O_2$ layered oxide without Mn^{3+} was synthesized successfully, which exhibited improved reversible specific capacity of 118 mAh/g in the voltage range of 2.4–4.0 V at 0.2 C, corresponding to the intercalation/deintercalation of 0.47 Na^+ (0.1 more than that of $Na_{0.90}Cu_{0.22}Fe_{0.30}Mn_{0.48}O_2$). This work demonstrates an important strategy to obtain advanced layered oxide cathodes for NIBs.

Keywords: copper redox, layered oxide, cathode, Na-ion batteries, energy storage

PACS: 82.47.–a, 82.45.Fk, 84.60.–h **DOI:** 10.1088/1674-1056/ac523b

1. Introduction

Li-ion batteries (LIBs) are the optimum choice for portable electronic devices and electric vehicles due to the high energy density and energy conversion efficiency. However, the energy density is not the primary consideration when it comes to large-scale or stationary electrical energy storage systems. Instead, Na-ion batteries (NIBs) as a helpful complement have drawn increasing interest owing to the abundance and low cost of sodium resources, as well as the similar Na^+ storage mechanism to that of the LIBs.[1,2] Extensive efforts have been made and improve the comprehensive performance of NIBs.[3–5] It is of great importance for the improvement of the performance of NIBs to explore electrode materials with high capacity, high voltage, and excellent cycle stability.[6,7] Layered transition metal (TM) oxides (Na_xTMO_2) are an important type of cathode materials due to their easy synthesis, remarkable Na^+ intercalation/deintercalation reversibility, excellent diffusion kinetics, and high theoretical capacity.[8–10] Driven by the urgent demand for electrode materials with high energy density, long-cycling stability and low-cost in the commercial application of NIBs, many cathode materials with superior electrochemical performance have been designed and developed in recent years.[6,11,12]

Cu^{2+} was firstly found to be electrochemically active in P2-$Na_{0.68}Cu_{0.34}Mn_{0.66}O_2$ compound.[13] Compared with other reported redox couple of $+2/+3$ valence in layered oxides, such as Ni^{3+}/Ni^{2+}, the advantage of Cu^{3+}/Cu^{2+} redox couple lies in its higher reaction potential and relatively low-cost. Subsequently, a series of Cu-containing layered oxides have been developed.[14–31] It was found that the Cu^{2+} substitution not only contributes to charge compensation,[14,15,17,20,21] but also improves cycling performance via suppressing phase transition,[22,23,25,26] or mitigating TM dissolution,[27,28] which enhance Na^+ diffusion kinetics and promote the rate performance of the cathode materials.[29–31] However, among the Cu-contained materials reported above, only part of the Cu^{3+}/Cu^{2+} redox couple participated in the redox reaction, and the activity of Cu^{3+}/Cu^{2+} redox for this type of materials needs to be further improved. The previous studies showed that Mg^{2+} substitution generally contributes to stabilizing the crystal structure. For example, $Na[Ni_{4/9}Mn_{1/3}Mg_{1/18}Ti_{1/6}]O_2$ goes through more continuous phase transitions and lattice parameter variation than the undoped one;[32] Mg dopant in O3-$NaMg_{0.05}[Ni_{1/3}Fe_{1/3}Mn_{1/3}]_{0.95}O_2$ suppresses the occurrence of irreversible phase transitions as well as structural degradation;[33] Mg doped P3-$Na_{2/3}Ni_{1/4}Mg_{1/12}Mn_{2/3}O_2$ is stable against water and air.[34] However, to date, there is yet to be a systematic study on the effect of Mg-doping on the electronic structure of the layered oxides cathode.

Compared with the P2-type layered oxides, the O3-type layered oxides have a considerably higher initial in-

†Corresponding author. E-mail: rong@iphy.ac.cn
‡Corresponding author. E-mail: yshu@iphy.ac.cn

© 2022 Chinese Physical Society and IOP Publishing Ltd

terlayer Na^+ content and thus can provide more reversible Na^+ de-intercalation and higher initial Coulombic efficiency. This is crucial for improving the reversible capacity of the Na-ion full-cell.[35] Herein, we report a novel Mg-doped O3-type Cu–Fe–Mn based layered oxide, O3-$Na_{0.90}Mg_{0.08}Cu_{0.22}Fe_{0.30}Mn_{0.40}O_2$ (abbreviated as NMCFM), with more reversible intercalation/deintercalation of Na^+ compared with undoped O3-$Na_{0.90}Cu_{0.22}Fe_{0.30}Mn_{0.48}O_2$ (abbreviated as NCFM).[36] This work reveals, for the first time, that Mg^{2+} doping could effectively promote the electrochemistry of the Cu^{3+}/Cu^{2+} redox, thus increasing the discharge voltage in O3-type materials. Based on the analysis of *in situ* x-ray diffraction (XRD) result, we found that the irreversible phase transition occurring at higher-voltage gives rise to the significantly increased polarization and capacity fading. By reducing the charge cutoff voltage to 3.85 V, we found that NMCFM still delivered a reversible capacity of 100 mAh/g with long-cycling stability.

2. Experimental details

2.1. Materials synthesis

The O3-$Na_{0.90}Mg_{0.08}Cu_{0.22}Fe_{0.30}Mn_{0.40}O_2$ and the referential sample O3-$Na_{0.90}Cu_{0.22}Fe_{0.30}Mn_{0.48}O_2$ were synthesized by a simple solid-state reaction at 850 °C in air atmosphere using precursors of Na_2CO_3 (Alfa, 99.5%), MgO (Aladdin, 99.9%), CuO (Aladdin, 99.9%), Fe_2O_3 (Aladdin, 99.8%), and MnO_2 (Aladdin, 99.5%).

2.2. Structure and morphology characterization

The XRD patterns were collected on a Bruker-AXS D8 Advance instrument using Cu $K\alpha$ radiation. The structural refinement was performed by Rietveld refinements using the Fullprof suite. The special cell for *in situ* XRD experiment during the first charge and discharge was assembled with the Al foil as the x-ray window and current collector. The actual chemical composition of the final materials was determined by inductively coupled plasma-atomic emission spectroscopy (ICP-AES, Shimadzu, ICPS-8100). Scanning electron microscopy (SEM) measurements were carried out on a Hitachi S-4800 (10 kV).

2.3. Electrochemical characterization

The working cathodes were fabricated by mixing active material with carbon nanotube and polytetrafluoroethylene (in a weight ratio of 8:1:1), which were rolled into thin films with the loading mass of the active material of 4–7 mg/cm^2. The prepared electrodes were dried at 100 °C under vacuum for 12 h and then were fabricated into CR2032 coin-type cells in an argon-filled glove box (H_2O, $O_2 < 0.1$ ppm). Commercial glass fibers and sodium metal were employed as the separator and counter/reference electrode, respectively. 1 M $NaClO_4$ in propylene carbonate/ethylene carbonate/dimethyl carbonate (PC/EC/DMC=1:1:1 in volume) with fluoroethylene carbonate (FEC, 2% in volume) was used as the electrolyte. The galvanostatic charge and discharge measurements were carried out on a Neware CT4000 battery test system in various voltage ranges and current rates under room temperature, and a rate of 1 C corresponding to 100 mA/g. The CV tests were performed on an electrochemical workstation CHI 760e in the voltage range of 2.4–3.9 V or 2.4–4.5 V vs. Na^+/Na at various scan rates. GITT was measured by applying the repeated current pulses for 30 min at a current density of 15 mA/g followed by relaxation for 2 h. The electrochemical impedance spectroscopy (EIS) of the coin cells was recorded by electrochemical workstation CHI 760e in the discharged state of 2.4 V at room temperature between 1 MHz and 10 mHz with an AC voltage of 5 mV.

3. Results and discussion

The Mg^{2+} doped NMCFM could be synthesized by means of solid-state reaction at 850 °C in air atmosphere. As shown in Fig. 1(a), NMCFM was characterized as a typical α-$NaFeO_2$ structure, belonging to the *R*-3*m* space group, similar to NCFM. A few weak diffraction peaks in XRD spectrum of NMCFM corresponded to CuO impurities. According to the XRD refinement result, part of the Mn^{3+} with a smaller ion radius was replaced by Mg^{2+} with a larger ion radius (0.62 Å vs. 0.72 Å). The lattice parameter $a = 2.96877$ Å increased while $c = 16.20971$ Å decreased comparing with the lattice parameter of NCFM ($a = 2.9587$ Å, $c = 16.3742$ Å). The ICP results confirmed that stoichiometric ratio of various elements was nearly the same as the designed one. Moreover, the chemical valence state of Mn in the material could be calculated to be +4 based on the electroneutrality principle. Evidently, the design objective material with free of Mn^{3+} was achieved, demonstrating that the Mg^{2+} was a good alternative to replace Mn^{3+}.

Furthermore, the size and morphology of NMCFM particles were studied by SEM, showing a particle size ranged from 1 μm to 3 μm. Meanwhile, almost all the particles were polyhedral and plate-like with smooth surfaces. Based on the energy dispersive spectroscopy (EDS) results (Fig. 1(b)), Cu, Fe, Mn and Mg elements were uniformly distributed in the material bulk, indicating that Mg ions were uniformly doped into NMCFM.

Galvanostatic charge–discharge test was carried out on NMCFM at a current rate of 0.2 C in Na-ion half-cells. The first-cycles of charging and discharging curves at different voltage intervals were compared, as shown in Fig. 2(a), showing that the initial Coulombic efficiency decreases as the charge cut-off voltage increases. In addition, the polarization

in a narrow voltage range is significantly reduced in comparison to that in a wider voltage window. It is possibly related to the irreversible migration of Fe^{4+} into the Na^+ layer upon increasing Fe^{3+}/Fe^{4+} redox reaction, which deteriorates the Na^+ diffusion dynamics.[20,37] Besides, when the charging voltage was above 4.0 V, a second voltage platform appeared, indicating another phase transformation occurred in the high-voltage range after the O3-P3 two-phase reaction. In consequence, both the reactions mentioned above may directly lead to the increase of polarization.

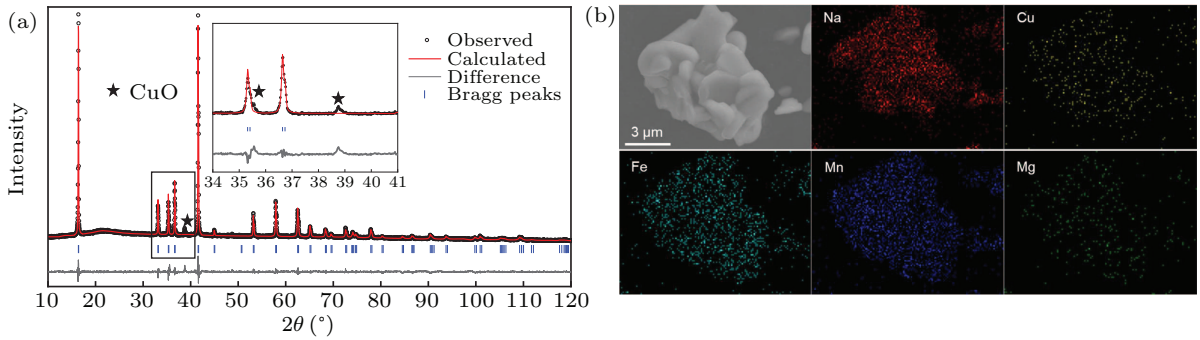


Fig. 1. Structural characterizations of NMCFM. (a) The XRD Rietveld refinement result of the sample; (b) SEM image and EDS mapping of the as-synthesized sample.

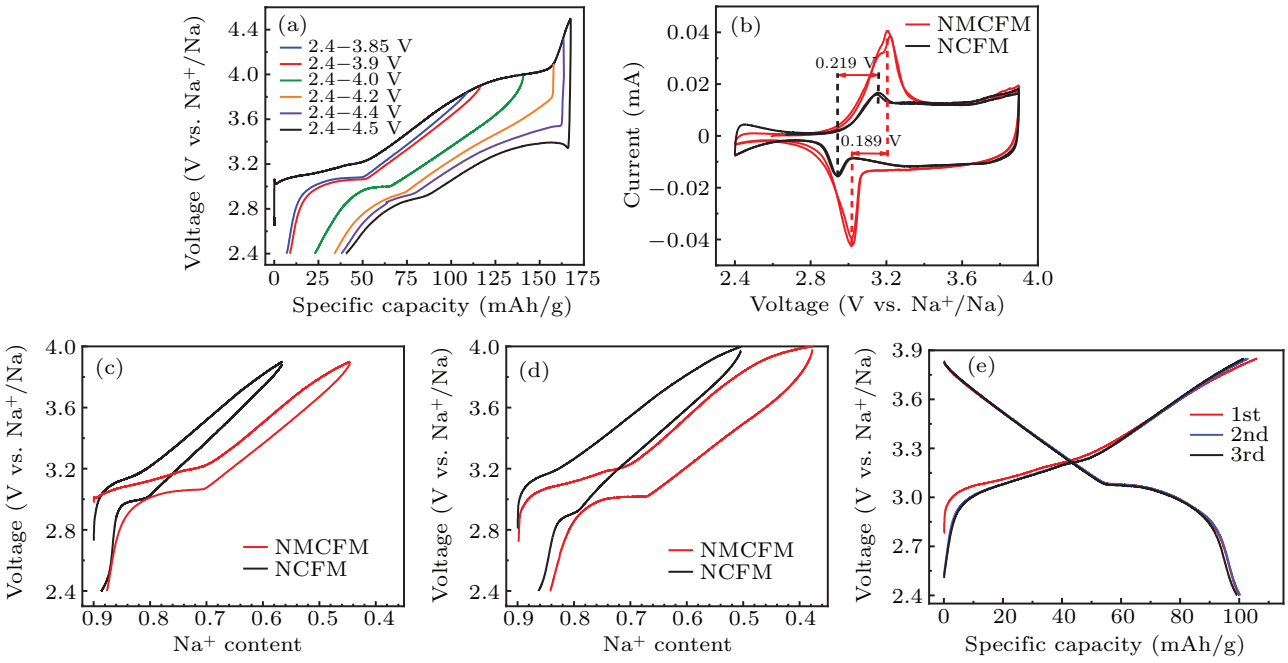


Fig. 2. The Na^+ storage performances of NMCFM and NCFM. (a) Galvanostatic charge–discharge curves of NMCFM electrodes at 0.1 C within different voltage ranges. (b) CV curves of NCFM and NMCFM electrodes. (c), (d) The initial charge–discharge curves of NCFM and NMCFM cathodes with voltage intervals of 2.4–3.9 V (c) and 2.4–4.0 V (d), respectively. (e) Charge–discharge curves of NMCFM cathode during the initial three cycle in the voltage interval of 2.4–3.85 V.

Cyclic voltammetry (CV) was employed to compare the kinetics property of these two oxide electrodes. As shown in Fig. 2(b), both oxide cathodes were tested with the potential ranges of 2.4–3.9 V using scan rates of 0.08 mV/s, demonstrating good reversibility in the first two cycles. A pair of reversible redox peaks (at 3.203 V and 3.014 V) are shown in the cyclic voltammogram of NCMFM, and a similar pair of reversible redox peaks (at 3.160 V and 2.941 V) are also displayed for NCFM. The redox peak potentials of NMCFM are higher than those of NCFM, indicating that Mg doping could increase the reaction potential of the oxide cathode. Furthermore, the electrochemical polarization (0.189 V) calculated between the redox peaks of NMCFM is also smaller than that of NCFM (0.219 V), indicating that Mg doping could enhance the phase stability as well.

It can be seen from Figs. 2(c) and 2(d), NMCFM delivers a reversible capacity of 107 mAh/g in the voltage range of 2.4–3.9 V, corresponding to the reversible intercalation/deintercalation of 0.43 Na^+, with high initial Coulombic efficiency of 92%. Whereas within the same voltage interval, NCFM only delivers a reversible capacity of 80 mAh/g, corresponding to the reversible intercalation/deintercalation of 0.32 Na^+. Similarly, in the voltage range of 2.4–4.0 V, NMCFM and NCFM respectively deliver a reversible capac-

ity of 117.7 mAh/g and 90 mAh/g, corresponding to the reversible intercalation/deintercalation of 0.47 and 0.37 Na^+ ions. Therefore, compared to NCFM, additional 0.10 Na^+ ions are available for NMCFM, resulting in the specific energy of 347.9 Wh/kg and 262.6 Wh/kg in the voltage range of 2.4–3.9 V, as well as 394.4 Wh/kg and 295.9 Wh/kg in the voltage range of 2.4–4.0 V for NMCFM and NCFM, respectively. As shown in Fig. 2(e), the NMCFM cathode can deliver a highly reversible capacity of ∼ 100 mAh/g in the voltage range of 2.4–3.85 V. As for the rate performances in the voltage range of 2.4–3.9 V, the reversible capacities of NMCFM are 107.3 mAh/g, 101.4 mAh/g, 93.3 mAh/g, 86.1 mAh/g, 79 mAh/g and 65 mAh/g at 0.1 C, 0.2 C, 0.5 C, 1 C, 2 C and 5 C (Fig. 3(a)), respectively. In comparison, the reversible capacities of NCFM are 88.1 mAh/g, 83.6 mAh/g, 77.3 mAh/g, 74.2 mAh/g, 71 mAh/g and 64.1 mAh/g at 0.1 C, 0.2 C, 0.5 C, 1 C, 2 C and 5 C (Fig. 3(b)), respectively. As a result, it could be concluded that Mg^{2+} doping contributes to the improvement of the electrochemical activity of Cu^{3+}/Cu^{2+} redox. Furthermore, as shown in Figs. 3(c)–3(d), NMCFM exhibited outstanding cyclability with capacity retention of 88% after 200 cycles at 0.2 C in 2.4–3.85 V; even at the higher rate of 1 C, 75% capacity was still retained after 500 cycles.[11]

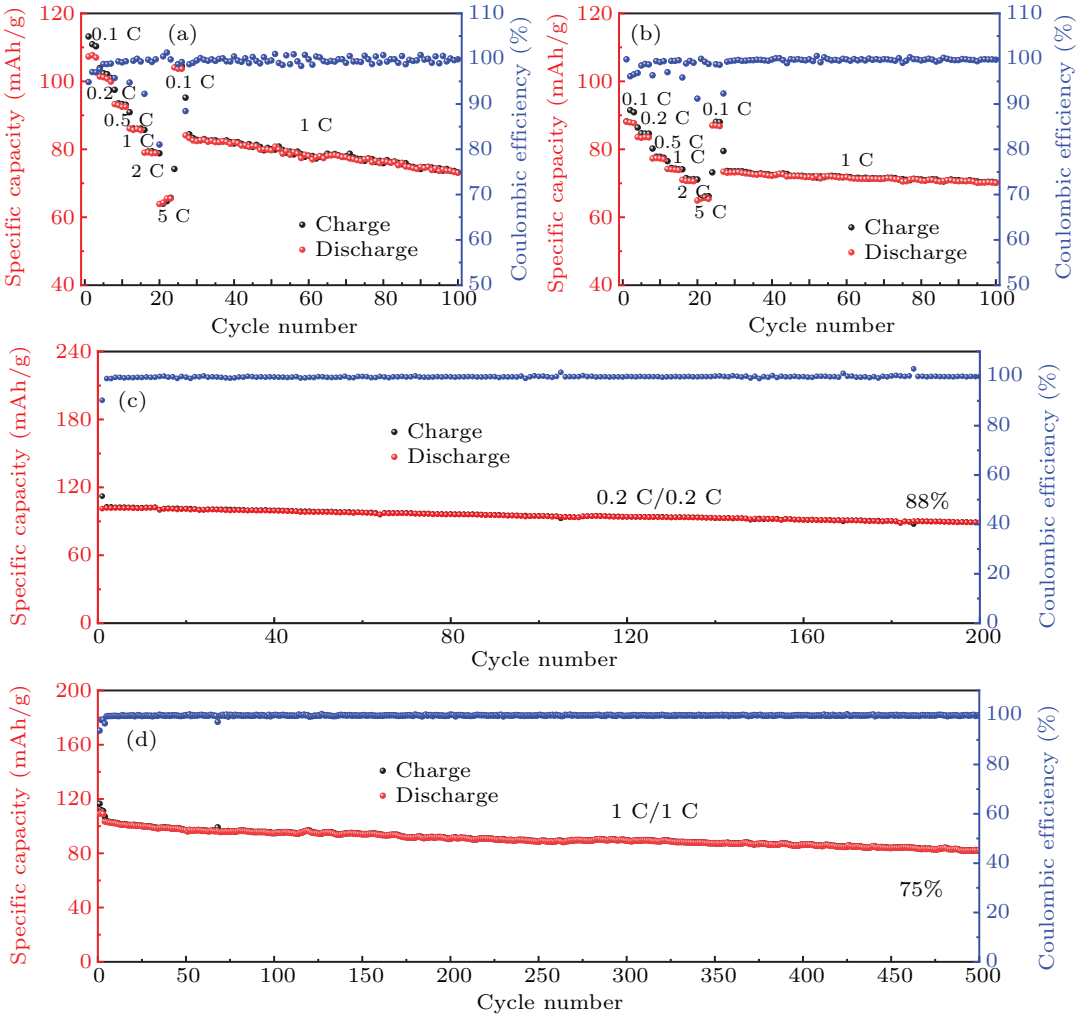


Fig. 3. Rate performance of NMCFM (a) and NCFM (b) cathodes in the voltage range of 2.4–3.9 V at various rates from 0.1 C to 5 C. Cycling performance of the NMCFM electrode with the voltage range of 2.4–3.85 V at 0.2 C (c) during 200 cycles, at 1 C (d) during 500 cycles.

In situ x-ray diffraction characterization was performed in order to capture the structural evolution process of NMCFM during the Na^+ insertion and extraction process. The corresponding *in situ* XRD spectra were collected during the initial charge and discharge process at the rate of 0.1 C in the voltage range of 2.4–4.0 V and are shown in Fig. 4. When Na^+ extraction amount x was lower than 0.1, or between 0.22 and 0.45, the material maintained O3 and P3 phase structures, respectively. Meanwhile, the diffraction peak (00l) shifted to a lower angle as the charging voltage increased. Evidently, along with the content of interlayered Na^+ decreased, the electrostatic repulsion between TMO_2 layers would increase, leading to an increase in the interlayer spacing along the c-axis. The single-phase solid solution reaction was consistent with electrochemical behavior in the corresponding interval of voltage. When the Na^+ extraction amount x was in the range from

0.12 to 0.22, the intensity of (003), (006) and (104) diffraction peaks that belonged to O3 phase declined gradually; in the meantime, the (003), (006) and (105) diffraction peaks that belonged to P3 phase started to appear, which implies O3 phase and P3 phase coexist in this process.[38] When the deintercalated Na^+ ion amount exceeded 0.45, the (00*l*) diffraction peaks moved towards a higher angle.[38] This might be due to the crystal structure starting to shrink upon the formation of more Na^+ vacancies. Furthermore, the (002) diffraction peak belonging to a new phase was found, which was identified as the OP2-like phase.[32] What is more, the intensities of various diffraction peaks dramatically decreased with peak-width broadening, which is due to a larger cubic deformation of OP2-like phase. Moreover, either the lattice distortion or the irreversible migration of Fe^{4+} to the Na^+ layer could hinder the Na^+ diffusion, which is consistent with the finding of the significant decline of D_{Na+} calculated by GITT. In short, during the initial charge process, the layered oxide cathode underwent the phase transformation of O3→P3→OP2-like, meanwhile the discharge process displayed an opposite phase transformation. However, when it was discharged to 2.4 V, the (003) diffraction peak angle of reformed O3 phase was lower than that of the pristine sample, which implies the Na^+ion content reduced slightly after the initial insertion and extraction cycle.

GITT is a common electrochemical technique that is used for analyzing the diffusion ability of Na^+ in electrode materials. As can be seen in Fig. 5(a), the apparent diffusion coefficient D_{Na+} is little changed in the voltage range of 2.4–3.9 V, reasonably maintaining at the 10^{-12} cm^2/s order of magnitudes.[39] However, D_{Na+} declines sharply in the voltage window ranged from 3.9 V to 4.5 V, which decreases to below 10^{-13} cm^2/s especially when it is charged to above 4.15 V. The reason is that Na^+ diffusion is severely hampered due to the generation of a new phase.[40] Furthermore, EIS of the fabricated coin cells consisting of NMCFM electrodes was measured and analyzed after the first cycle in the voltage ranges of 2.4–3.85 V and 2.4–4.5 V, respectively. It is obvious that the electrode cycled in the voltage range of 2.4–3.85 V exhibits lower resistance than the electrode cycled in the voltage range of 2.4–4.5 V, suggesting the reduced Na^+ diffusion resistance and charge-transfer resistance when cycled in narrow voltage range. These results suggest that Mg^{2+} doping stabilizes the layered structures in a suitable voltage range, thus enhancing the electrochemical properties of the layered oxides. Our findings from the systematic studies on the influence of doping metal are instructive and will stimulate further research for enhancing the structural stability and electrochemical performance of the O3-type layered oxide cathode at higher voltages.

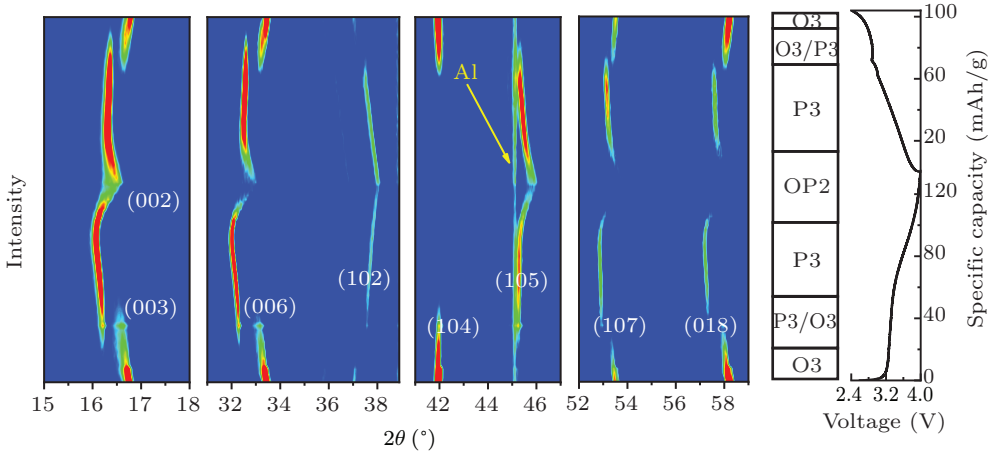


Fig. 4. *In situ* XRD patterns collected for the initial charge and discharge process at the rate of 0.1 C in the voltage interval between 2.4–4.0 V of NMCFM in Na-ion half-cell. Corresponding phase evolution and capacity–voltage curves are illustrated on the right side.

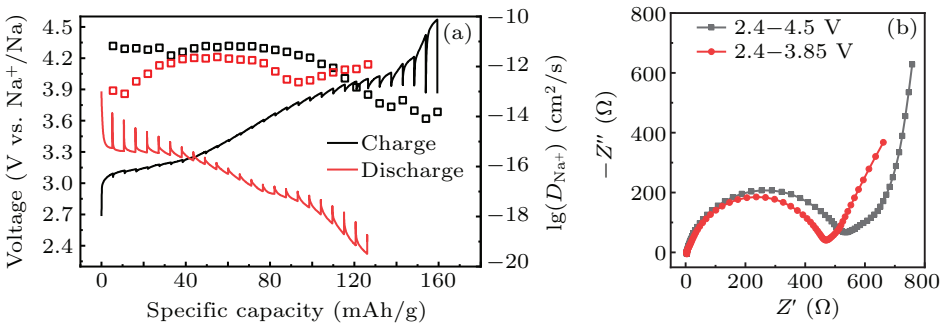


Fig. 5. (a) GITT curves and diffusion coefficient D_{Na+} of the NMCFM cathode with voltage interval of 2.4–4.5 V for the initial charge and discharge cycle. (b) EIS of the NMCFM electrodes after the first cycle in the voltage interval of 2.4–3.85 V and 2.4–4.5 V, respectively.

We also assembled full cells with hard carbon (HC) as the anode to demonstrate the excellent electrochemical performance of the NMCFM cathode. Figures 6(a) and 6(b) show that a reversible storage capacity of ∼ 92 mAh/g (based on the mass of cathode active material in the cell) was achieved in the voltage range of 0.5–3.85 V at 0.1 C. The specific energy density was calculated to be 262 Wh/kg based on the total mass of cathode and anode active materials. The reversible capacities were 70 mAh/g and 47 mAh/g at the rates of 2 C and 5 C (Fig. 6(a)), respectively. The cell also presented excellent cycling stability and the capacity retention was 96% after 80 cycles at 1 C rate. Thus, the high energy density and cycle stability revealed in the full cells stand a good chance to meet the practical applications and commercial demands henceforward.

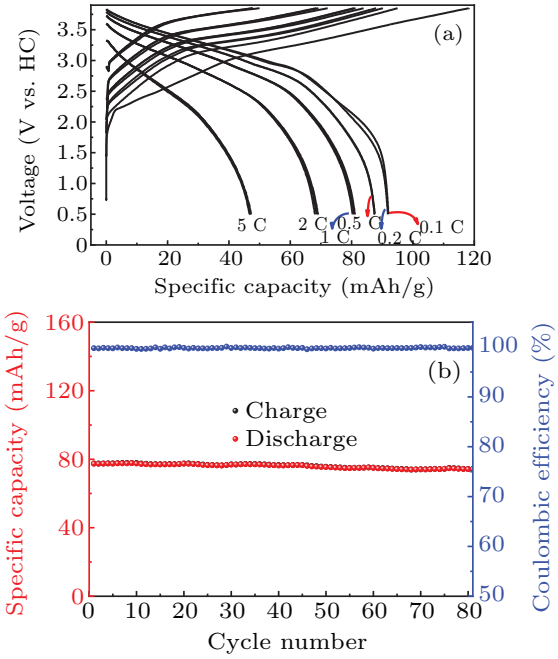


Fig. 6. Electrochemical performance of the NMCFM//hard carbon full cells: (a) charge/discharge curves in the voltage range of 0.5–3.85 V at different rates and (b) the cycling performance at 1 C.

4. Conclusions

In summary, we reported an O3-type Mg^{2+}-doped NMCFM ($Na_{0.90}Mg_{0.08}Cu_{0.22}Fe_{0.30}Mn_{0.40}O_2$) cathode material without Mn^{3+}. The XRD and ICP results indicated that Mg^{2+} is a good alternative to replace Mn^{3+}, which is helpful to increase the reversible specific capacity. Both the SEM and EDS results further illustrated the doped element Mg^{2+} was distributed uniformly. The *in situ* XRD data demonstrated a reversible O3→P3→OP2-like phase→P3→O3 transformation during the initial charge and discharge process in the voltage range of 2.4–4.0 V. Combined with the GITT analysis, the formation of OP2-like phase at high voltage probably contributes to the reduction of D_{Na+}, leading to the reversibility of Na^+ intercalation/deintercalation fading eventually. In the voltage range of 2.4–4.0 V, NMCFM delivered a reversible capacity of 118 mAh/g at 0.2 C, which is significantly higher than that of undoped NCFM. Through limiting the voltage within 2.4–3.85 V, the NMCFM cathode exhibited the capacity retention of 88% after 200 cycles at 0.2 C, 75% after 500 cycles at 1 C. As a result, considering the involvement of Cu^{3+}/Cu^{2+} redox couple in the charge/discharge process, it can be concluded that Mg^{2+} doping contributes to improve the electrochemical activity of Cu^{3+}/Cu^{2+}. In full cells, it provides a reversible storage capacity of around ∼ 92 mAh/g, achieving a specific energy density of 262 Wh/kg with the capacity retention of 96% after 80 cycles at the rate of 1 C. The NMCFM with high specific capacity and good cycling stability stands a good chance to meet the practical applications and commercial demands henceforward.

Acknowledgements

Project supported by the National Natural Science Foundation of China (Grant Nos. 51725206, 52122214, and 52072403), the Strategic Priority Research Program of the Chinese Academy of Sciences (Grant No. XDA21070500), Youth Innovation Promotion Association of the Chinese Academy of Sciences (Grant No. 2020006), and Beijing Municipal Natural Science Foundation, China (Grant No. 2212022).

References

[1] Liu Q, Hu Z, Li W, Zou C, Jin H, Wang S, Chou S and Dou S X 2021 *Energ. Environ. Sci.* **14** 158
[2] Zhou Q, Li Y, Tang F, Li K, Rong X, Lu Y, Chen L and Hu Y S 2021 *Chin. Phys. Lett.* **38** 076501
[3] Fatima H, Zhong Y, Wu H and Shao Z 2021 *Mater. Rep. Energy* **1** 100022
[4] Yang C, Xin S, Mai L and You Y 2020 *Adv. Energy Mater.* **11** 2000974
[5] Zhao C, Lu Y, Chen L and Hu Y S 2019 *InfoMat* **2** 126
[6] Li C, Geng F, Hu B and Hu B 2020 *Mater. Today Energy* **17** 100474
[7] Guo H, Sun K, Lu Y, Wang H, Ma X, Li Z, Hu Y S and Chen D 2019 *Chin. Phys. B* **28** 068203
[8] Palaniyandy N 2020 *Curr. Opin. Electroche.* **21** 319
[9] Liu H, Deng W, Gao X, Chen J, Yin S, Yang L, Zou G, Hou H and Ji X 2020 *Nano Sel.* **1** 200
[10] Ren M, Fang H, Wang C, Li H and Li F 2020 *Energ. Fuel* **34** 13412
[11] Ding F, Meng Q, Yu P, Wang H, Niu Y, Li Y, Yang Y, Rong X, Liu X, Lu Y, Chen L and Hu Y S 2021 *Adv. Funct. Mater.* **31** 2101475
[12] Hu Y S and Li Y 2021 *ACS Energy Lett.* **6** 4115
[13] Xu S Y, Wu X Y, Li Y M, Hu Y S and Chen L Q 2014 *Chin. Phys. B* **23** 118202
[14] Gao X, Chen J, Liu H, Yin S, Tian Y, Cao X, Zou G, Hou H, Wei W, Chen L and Ji X 2021 *Chem. Eng. J.* **406** 126830
[15] Yang L, Luo S H, Wang Y, Zhan Y, Wang Q, Zhang Y, Liu X, Mu W and Teng F 2021 *Chem. Eng. J.* **404** 126578
[16] Chen S, Han E, Xu H, Zhu L, Liu B, Zhang G and Lu M 2017 *Ionics* **23** 3057
[17] Wang P F, Xiao Y, Piao N, Wang Q C, Ji X, Jin T, Guo Y J, Liu S, Deng T, Cui C, Chen L, Guo Y G, Yang X Q and Wang C 2020 *Nano Energy* **69** 104474
[18] Yan Z, Tang L, Huang Y, Hua W, Wang Y, Liu R, Gu Q, Indris S, Chou S L, Huang Y, Wu M and Dou S X 2019 *Angew Chem. Int. Ed. Engl.* **58** 1412
[19] Ramasamy H V, Kaliyappan K, Thangavel R, Aravindan V, Kang K, Kim D U, Park Y, Sun X and Lee Y S 2017 *J. Mater. Chem. A* **5** 8408

[20] Xu S, Wu J, Hu E, Li Q, Zhang J, Wang Y, Stavitski E, Jiang L, Rong X, Yu X, Yang W, Yang X Q, Chen L and Hu Y S 2018 *J. Mater. Chem. A* **6** 20795

[21] Fu F, Liu P and Wang H 2019 *Mater. Lett.* **253** 124

[22] Luo R, Zhang N, Wang J, Qu W, Li L, Wu F and Chen R 2021 *Electrochim. Acta* **368** 137614

[23] Zhang X, Qiu F, Jiang K, He P, Han M, Guo S and Zhou H 2020 *Chem. Commun.* **56** 6293

[24] Deng J, Luo W B, Lu X, Yao Q, Wang Z, Liu H K, Zhou H and Dou S X 2018 *Adv. Energy Mater.* **8** 1701610

[25] Xiao Y, Zhu Y F, Yao H R, Wang P F, Zhang X D, Li H, Yang X, Gu L, Li Y C, Wang T, Yin Y X, Guo X D, Zhong B H and Guo Y G 2019 *Adv. Energy Mater.* **9** 1803978

[26] Zhao Q, Butt F K, Yang M, Guo Z, Yao X, Zapata M J M, Zhu Y, Ma X and Cao C 2021 *Energy Storage Mater.* **41** 581

[27] Kong W, Gao R, Li Q, Yang W, Yang J, Sun L and Liu X 2019 *J. Mater. Chem. A* **7** 9099

[28] Hu G, Liu Y, Li W, Peng Z, Wu J, Xue Z, Shi Y, Fan J, Sun Q, Cao Y and Du K 2020 *Ionics* **27** 657

[29] Wang Y, Kim S, Lu J, Feng G and Li X 2020 *Batteries Supercaps* **3** 376)

[30] Xu J, Chen J, Zhang K, Li N, Tao L and Wong C P 2020 *Nano Energy* **78** 105142

[31] Dang R, Li Q, Chen M, Hu Z and Xiao X 2018 *Phys. Chem. Chem. Phys.* **21** 314

[32] Kubota K, Fujitani N, Yoda Y, Kuroki K, Tokita Y and Komaba S 2021 *J. Mater. Chem. A* **9** 12830

[33] Jung K N, Choi J Y, Shin H S, Huu H T, Im W B and Lee J W 2020 *Solid State Sci.* **106** 106334

[34] Zhang C, Gao R, Zheng L, Hao Y and Liu X 2018 *ACS Appl. Mater. Inter.* **10** 10819

[35] Zhao C, Wang Q, Yao Z, Wang J, Sánchez-Lengeling B, Ding F, Qi X, Lu Y, Bai X and Li B 2020 *Science* **370** 708

[36] Mu L, Xu S, Li Y, Hu Y S, Li H, Chen L and Huang X 2015 *Adv. Mater.* **27** 6928

[37] Yabuuchi N, Yoshida H and Komaba S 2012 *Electrochemistry* **80** 716

[38] Komaba S, Yabuuchi N, Nakayama T, Ogata A, Ishikawa T and Nakai I 2012 *Inorg. Chem.* **51** 6211

[39] Gu Z Y, Guo J Z, Zhao X X, Wang X T, Xie D, Sun Z H, Zhao C D, Liang H J, Li W H and Wu X L 2021 *InfoMat* **3** 694

[40] Ding F, Zhao C, Zhou D, Meng Q, Xiao D, Zhang Q, Niu Y, Li Y, Rong X, Lu Y, Chen L and Hu Y S 2020 *Energy Storage Mater.* **30** 420